Earth, Planets and Space

FULL PAPER Open Access

Occurrence and controls of ~ 1 Hz waves in Mercury's magnetosphere: insights from MESSENGER observations

M. Persson[1*], A. P. Dimmock[1], J.-E. Wahlund[1], M. Morooka[1], E. Yordanova[1], A. I. Eriksson[1], L. Z. Hadid[2], S. Aizawa[2], Yu. V. Khotyaintsev[1], N. J. T. Edberg[1] and M. André[1]

Abstract

Mercury's magnetosphere is highly dynamic, with processes occurring on much shorter spatial and temporal scales than at Earth due to its weak magnetic field and proximity to the Sun. Wave-driven transport of energy and momentum is a key manifestation of these dynamics. We present a comprehensive statistical survey of ~ 1 Hz waves using the full MESSENGER magnetometer dataset. These waves occur on average 10–20% of the time within Mercury's magnetosphere, predominantly on closed field lines. Their occurrence is enhanced under conditions that favour an expanded closed field region, such as a northward interplanetary magnetic field or low internal magnetospheric disturbance. Wave power peaks in the post-midnight sector, mirroring asymmetries seen in other plasma parameters and suggesting a generation mechanism linked to particle injections along closed field lines near the magnetic equator. While the precise wave mode is not determined here, their frequency range, polarization, and occurrence context are broadly consistent with electromagnetic ion cyclotron-like waves. These results provide the first global characterization of ~ 1 Hz waves and their dependence on upstream and internal conditions, establishing a foundation for interpreting future BepiColombo observations and for understanding wave-driven dynamics in Mercury's magnetosphere.

Keywords Mercury, Magnetosphere, Ion scale waves, Dipolarisation fronts

*Correspondence:
M. Persson
moa.persson@irf.se
Full list of author information is available at the end of the article

© The Author(s) 2026. **Open Access** This article is licensed under a Creative Commons Attribution 4.0 International License, which permits use, sharing, adaptation, distribution and reproduction in any medium or format, as long as you give appropriate credit to the original author(s) and the source, provide a link to the Creative Commons licence, and indicate if changes were made. The images or other third party material in this article are included in the article's Creative Commons licence, unless indicated otherwise in a credit line to the material. If material is not included in the article's Creative Commons licence and your intended use is not permitted by statutory regulation or exceeds the permitted use, you will need to obtain permission directly from the copyright holder. To view a copy of this licence, visit http://creativecommons.org/licenses/by/4.0/.

Graphical Abstract

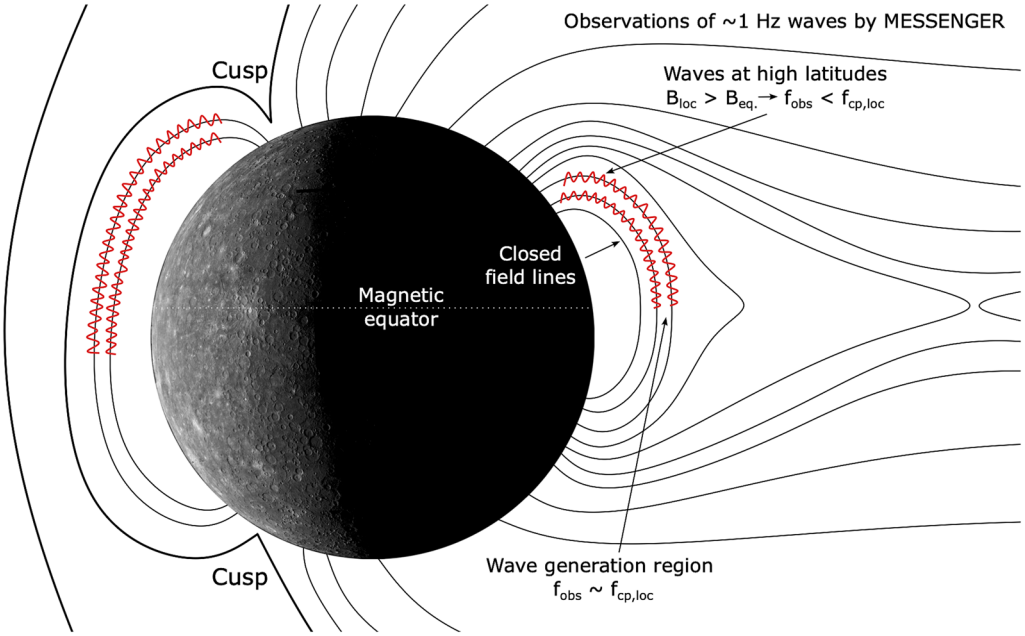

1 Introduction

Mercury's magnetosphere is a highly dynamic environment, hosting a variety of plasma processes despite its small size. Observations from the MESSENGER mission revealed that the magnetosphere is populated primarily by solar wind protons, with a smaller contribution from heavy ions originating from Mercury's tenuous and variable exosphere (Raines et al. 2013). The planet's intrinsic magnetic field is weak compared to Earth's, with a dipole moment of 195 nT R_M^3 (R_M = 2440 km, Mercury radius), and its dipole centre shifted northward by roughly 484 km (Alexeev et al. 2010; Anderson et al. 2012, 2010). The combination of the weak intrinsic field and the planet's proximity to the Sun, where the solar wind dynamic pressure at Mercury is higher than at any other planet in the solar system, results in a highly compressed magnetosphere. The subsolar magnetopause distance varies from the mean distance of 1.45 R_M to, in extreme cases, below the planetary surface (Jia et al. 2019; Slavin et al. 2019; Winslow et al. 2013; Zhong et al. 2015). Within the closed field regions, Mercury hosts quasi-trapped ion populations that drift along magnetic field lines, but, unlike at Earth, they often do not complete full drift orbits before impacting the surface or escaping the magnetosphere (Schriver et al. 2011; Trávníček et al. 2010; Zhao et al. 2022a). The interaction of the solar wind with Mercury's magnetic field and surface also drives substorm-like phenomena analogous to those at Earth, but without a conductive ionosphere (e.g. Slavin et al. 2021, 2018, 2010). Consequently, the solar wind strongly controls both the magnetospheric dynamics and the direct plasma-surface interaction. As the only magnetosphere that can be studied in situ in close proximity to a main-sequence star, Mercury provides a unique opportunity to investigate fundamental plasma processes and to place magnetospheric dynamics in a broader solar system context.

As Mercury's magnetosphere is small, rapidly evolving, and weakly shielded from the solar wind, wave–particle interactions are expected to play a significant role in controlling plasma dynamics. Wave activity is a key indicator of energy redistribution in collisionless magnetospheric plasmas, mediating the transfer of energy between particles and fields and regulating plasma stability. Consistent with these expectations, a wide variety of wave phenomena has been observed within Mercury's magnetosphere. Upstream of the bow shock, the foreshock region generates ultra-low-frequency (ULF) waves that can penetrate through the bow shock and into the magnetosheath (Jarvinen et al. 2020; Romanelli et al. 2020). Occasionally these waves may further penetrate into the magnetosphere across the magnetopause (Kallio et al. 2022; Liljeblad et al. 2016; Liljeblad and Karlsson 2017). The magnetopause itself is frequently subject to the

Kelvin–Helmholtz instability (KHI), which is observed more often on the dusk than the dawn flank (Liljeblad et al. 2014). Within the magnetosphere, Alfvénic and compressional waves at 0.01–0.1 Hz, analogous to the Pi2 pulsations at Earth, have been linked to the substorm expansion phases and can carry field-aligned current pulses along the magnetic field, connecting the magnetotail to the nightside polar regions and providing information about magnetotail reconfigurations (Sun et al. 2015). ULF waves below 0.05 Hz are also seen to have a preference for the dayside magnetopause and the nightside plasma sheet (James et al. 2016) and may be driven by magnetopause instabilities such as KHI (Liljeblad et al. 2016, 2014).

Among the observed wave phenomena, waves near ~ 1 Hz, occurring close to the local ion cyclotron frequency, are of particular interest because of their potential to resonate with local ions and thereby directly influence ion dynamics through wave–particle interactions. Early MESSENGER observations showed that such coherent waves near ~ 1 Hz are common in Mercury's magnetosphere, with maximum power near the equatorial plane, where they also tend to be more compressional compared to higher latitudes (Boardsen et al. 2012). They occurred more frequently in the pre-midnight than in the post-midnight sector, and often had wave frequencies close to or below the local proton cyclotron frequency, while simultaneously often showing wave peaks at several harmonics above. These waves have been interpreted as either electromagnetic ion cyclotron (EMIC) waves or electromagnetic ion Bernstein mode waves (Boardsen et al. 2015). Correlations between wave power and proton flux modulations (Zhao et al. 2022b) and between the wave activity and KH waves or proton phase space density gradients (Li et al. 2025) suggest coupling between these wave modes and global dynamics. In addition, analysis of two MESSENGER flybys demonstrated that ~ 1 Hz waves are present under markedly different upstream solar wind conditions, while exhibiting substantial variability in wave power (Boardsen et al. 2009). This suggests that ~ 1 Hz wave activity is a persistent feature of Mercury's magnetosphere, but that its characteristics are sensitive to the global magnetospheric configuration.

As Mercury's magnetosphere responds strongly to changes in the interplanetary magnetic field (IMF), variations in upstream conditions could be expected to influence the occurrence and properties of the wave activity in the magnetosphere. The IMF orientation governs dayside reconnection, flux transport, and asymmetries in plasma distributions (Imber and Slavin 2017; Korth et al. 2011b; Slavin et al. 2012). A southward IMF may enhance dayside reconnection and magnetospheric openness, whereas northward IMF produces a more closed configuration, which has effects on the reconnection rates and the rate of solar wind entry into the magnetosphere (DiBraccio et al. 2013; Fatemi et al. 2020; Lavorenti et al. 2023). A strong B_Y component can generate dawn–dusk asymmetries (Tenfjord et al. 2015), and the B_X polarity determines which hemisphere dominates dayside reconnection (Cowley 1981; Lockwood et al. 2017). Moreover, the IMF direction defines the foreshock geometry and magnetosheath dynamics, which can modulate the wave environment near the magnetopause (Jarvinen et al. 2020; Liljeblad et al. 2016; Romanelli et al. 2020). These effects together imply that the IMF variability may modulate the ~ 1 Hz wave activity, especially if its generation mechanisms are linked to solar wind, magnetosheath, or foreshock conditions upstream of the magnetosphere, as well as reconnection activity inside the magnetosphere, yet these potential connections have not been tested statistically.

Despite more than a decade since the MESSENGER observations, our understanding of ~ 1 Hz wave activity at Mercury remains fragmented. Previous studies have established that these waves are common, spatially structured, and sometimes linked to ion dynamics, but they have largely relied on limited orbital subsets, selected events, or focused on wave identification and classification rather than a systematic assessment of global occurrence and upstream control. As a result, while ~ 1 Hz waves are known to occur frequently, it remains unclear how their global occurrence and properties vary across Mercury's magnetosphere and with upstream and magnetospheric conditions. Establishing where and under which conditions these waves occur is a necessary first step towards understanding their physical role in redistributing energy in Mercury's magnetosphere.

Here, we provide the first analysis of the complete set of full time resolution MESSENGER magnetometer data in order to quantify the occurrence and properties of these waves, providing essential context for interpreting BepiColombo's future observations. We focus on the statistical distribution of the ~ 1 Hz waves and their dependence on upstream conditions, providing an initial physical interpretation of their occurrence.

A detailed assessment of their wave mode (beyond Boardsen et al. 2015, 2012) and correlations with particle measurements is beyond the scope for this study, but represents a natural next step. The arrival of BepiColombo (Benkhoff et al. 2021) in late 2026, equipped with a comprehensive set of electric and magnetic field, and plasma instruments, and two spacecraft that cover some of the same plasma measurements, will enable unprecedented investigations of wave–particle interactions and magnetospheric dynamics at Mercury. The statistics established here provide essential context for interpreting

these upcoming observations and for identifying when and where targeted multi-instrument studies are more effective.

This paper is structured as follows: Sect. 2 describes the instrumentation and analysis methods, Sect. 3 presents the statistical results of wave properties and occurrence, Sect. 4 compares our findings with previous studies and discusses implications for wave modes and generation mechanisms, Sect. 5 outlines the perspectives for Bepi-Colombo, and Sect. 6 summarizes the main conclusions.

2 Instrumentation and methods

This study uses magnetic field data from the fluxgate magnetometer (MAG) onboard the MESSENGER spacecraft (Solomon et al. 2007). MESSENGER orbited Mercury from March 2011 to April 2015, completing over 4000 orbits. All intervals with high-resolution data are included. Inside the magnetosphere, MAG operated at a sampling frequency of 20 samples per second, allowing investigation of magnetic fluctuations up to ~ 10 Hz (Anderson et al. 2007). Mercury's smaller size and weaker magnetic field shift characteristic plasma frequencies downward compared to Earth, making ion-scale waves accessible in the 0.05–10 Hz range (Boardsen et al. 2012).

Magnetic field vectors are transformed into a mean-field-aligned (MFA) system (Schmid et al. 2021). The mean background field is obtained using a 0.01 Hz low-pass Butterworth filter, corresponding to a characteristic timescale of ~ 100 s. This timescale is long compared to the ~ 1 Hz wave activity studied here, while remaining short enough to follow the rapidly varying background magnetic field as seen by MESSENGER. The parallel component is along this background field and is detrended by removing the mean background field strength, the first perpendicular component is defined by the cross product between the parallel direction and the Z-axis of the Mercury Solar Orbital (MSO) coordinate system, and the second perpendicular component completes the right-handed orthogonal system. MSO is Mercury-centric and defined with X pointing Sunward, Z along Mercury's north orbital pole, and Y completing the right-handed system. Here, the analysis focuses on the parallel and total perpendicular components of the wave power, and does not rely on the specific orientation of the two perpendicular directions. Therefore, the adopted MFA definition is sufficient for the purposes of this study.

Wave properties are analysed using wavelet spectral methods. Continuous wavelet transforms (Torrence and Compo 1998) are applied to the MFA components to identify the dominant wave power as a function of frequency and time, generating a power spectral density matrix. Polarization properties, including compressibility, ellipticity, and degree of polarization, are derived following the Means method (Means 1972) on narrowband intervals around identified wave frequencies in the spacecraft frame. Figure 1 shows an example orbit on 15 September 2011, where the ~ 1 Hz waves are observed in both the dayside and nightside portion of the orbit, together with the zoomed in parts of both sides. In addition to the dominant spectral peak near ~ 1 Hz, one or more harmonic peaks at higher frequencies are visible. Such harmonic structure has been discussed in previous studies (e.g. Boardsen et al. 2015). In the present study, however, we focus exclusively on the primary ~ 1 Hz peak, and the harmonics are not included in the statistical analysis.

Wave events are identified semi-manually by visual inspection of the wavelet spectra, focusing on coherent ridge-like structures in the 0.5–5 Hz frequency range. In contrast to approaches that integrate power over a fixed frequency band, we require the presence of a temporally and spectrally coherent ridge. The ridge frequency may drift upward or downward in time and may temporarily extend beyond this nominal range, which are included provided coherence is maintained.

(See figure on next page.)

Fig. 1 Example of a ~ 1 Hz wave event observed by MESSENGER on 15 September 2011. The heliocentric distance (R_H), true anomaly angle (TAA; the angle of Mercury along its orbit measured from perihelion), and disturbance index (MDI) at pericentre are shown at the top. **a**, **b** Magnetic field in MSO and MFA coordinates, where the MFA parallel component is detrended by removing the mean background magnetic field. **c**, **d** Wavelet power spectral density of the parallel ($P_{\parallel}$) and perpendicular ($P_{\perp} = P_{\perp 1} + P_{\perp 2}$) magnetic components. White dashed lines mark the cyclotron frequencies of H^+, He^+, Na^+, and K^+ (top to bottom), and the white arrows in panel **c** mark the start (upward pointing) and end (downward pointing) of the identified ~ 1 Hz waves for this orbit. **e**–**g** MESSENGER trajectory in MSO coordinates projected onto the X–Y, X–Z, and Y–Z planes. Average magnetospheric boundaries (Winslow et al. 2013) are shown as dashed grey curves; blue and red dots mark bow shock and magnetopause crossings identified by Sun (2023). Colour along the trajectory indicates time, from light to dark. **h**, **i**, **k**, **l** MSO and MFA magnetic field components for the two time intervals marked by black dashed lines in panels **a**–**d**. **j**, **m** Fast Fourier Transform spectra for the same intervals showing parallel (blue) and perpendicular (orange) components. Black arrows mark the main peaks at ~ 1 Hz, which for both intervals are left-hand polarized waves with a wave vector angle to the magnetic field of about 60°. Solid black lines indicate the average proton gyrofrequency, with the dashed lines indicate its range during each interval. Harmonic structures above the local proton cyclotron frequency are visible in both cases, but are not included in this study

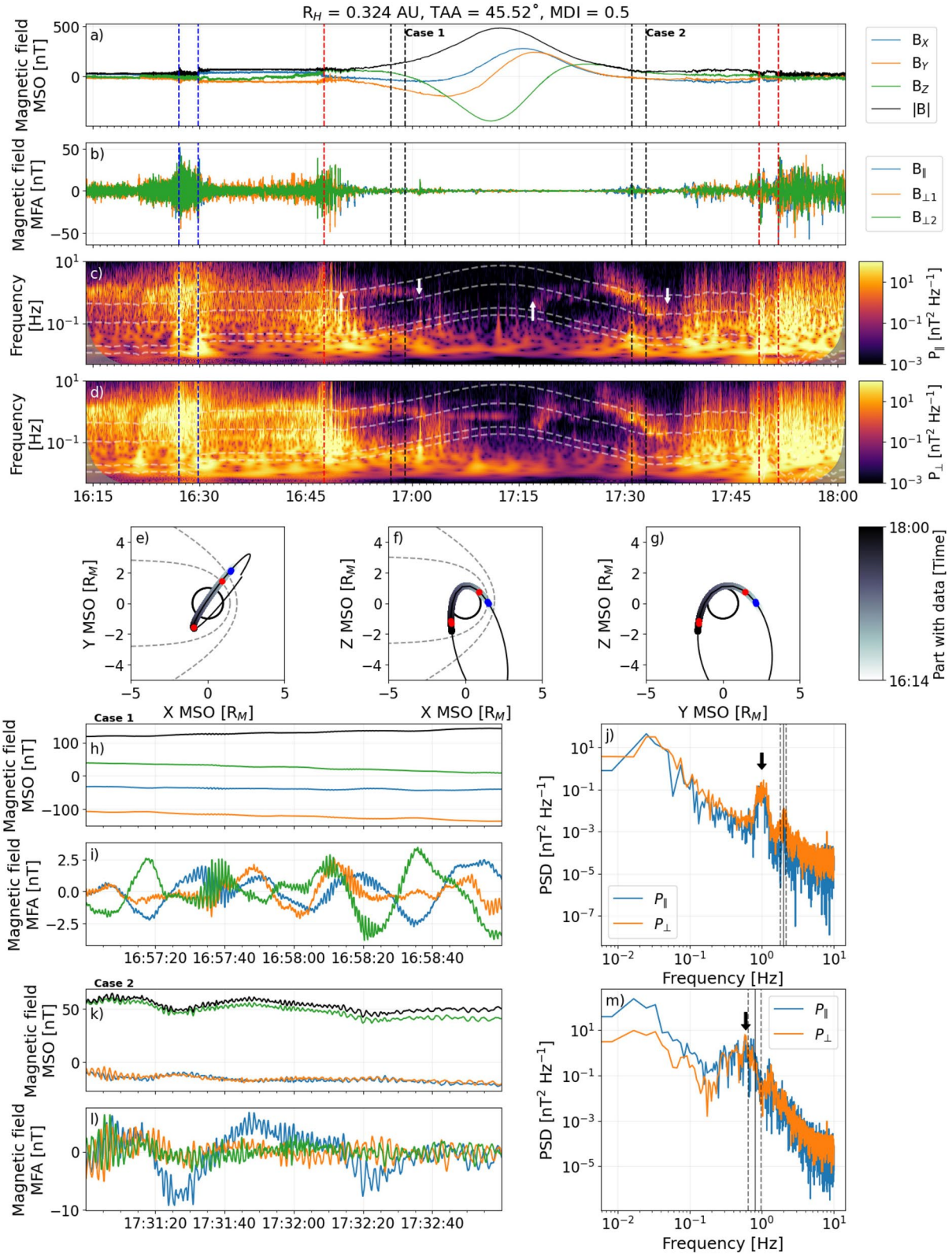

Fig. 1 (See legend on previous page.)

For each identified ridge, the approximate peak frequency and time interval are first defined. The instantaneous peak frequency is then determined at each time step by locating the maximum power spectral density within a narrow frequency window centred on the ridge, thereby avoiding spurious frequency jumps. Wave properties (e.g. compressibility, degree of polarization) are calculated at this tracked peak frequency. Events are retained only if they exhibit a clear power enhancement above the background level, exceed 0.01 nT^2 Hz^{-1} in spectral power, and have a degree of polarization above 0.9. This threshold is well above the estimated instrument noise floor (~ 10 pT^2 Hz^{-1}; Anderson et al. 2007). These criteria ensure that the statistics reflect discrete, coherent wave packets and minimize contamination from instrumental noise or broadband turbulent fluctuations.

In this study, we do not attempt to determine the specific wave mode of these ~ 1 Hz waves. Boardsen et al. (2015) concluded, using ray tracing simulations, that such waves are consistent with EMIC or electromagnetic ion Bernstein waves, likely generated by loss-cone plasma distributions on closed field lines near Mercury's magnetic equator. However, the limitations of single spacecraft magnetometer measurements prevent a definitive mode identification. While a discussion of the possible wave modes is provided in Sect. 4, the primary objective of this work is not mode discrimination but to quantify the spatial occurrence and large-scale statistical behaviour of these narrowband wave events. The statistical occurrence and spatial distribution of the ~ 1 Hz waves provide important constraints on their generation mechanisms. For these purposes, identifying robust spectral peaks near ~ 1 Hz with coherent polarization properties is valuable. The upcoming BepiColombo mission, with its multi-instrument and multi-spacecraft measurements, will be better suited to conclusively address the inherent wave nature.

Upstream conditions are determined from MAG measurements outside the bow shock. Bow shock crossings are obtained from Sun (2023), and for orbits not included in that dataset the average bow shock location from Winslow et al. (2013) is used. For each orbit, the average IMF strength, clock angle, and cone angle are calculated using intervals 20 min upstream the inbound and outbound bow shock crossings, and an average value between the two is used for each orbit. The choice of a 20-min interval is motivated by previous statistical studies showing that the IMF at Mercury's orbit typically maintains a relatively stable orientation for ~ 20 min (James et al. 2017). This interval is long enough to provide a representative estimate of the upstream IMF while short enough to limit the influence of longer-term solar wind variations and short-term fluctuations. The separation in time between the IMF interval and the observation of the ~ 1 Hz waves, along with temporal variations within the averaging interval, could influence individual data points. However, given the large number of orbits analysed in this study, the statistical trends reported here remain robust. The clock angle is defined as 0° for purely northward IMF (along Z_{MSO}) and 90° for along Y_{MSO}. The cone angle is measured relative to the MSO X-axis, with 0° when pointing purely Sunward. The distributions of the calculated IMF parameters (not shown) are in good agreement with earlier statistical analyses at Mercury (James et al. 2017), indicating that the derived upstream conditions provide a reliable basis for the statistical trends presented in this study.

The MESSENGER disturbance index (MDI) used in this study is taken directly from the dataset published by Anderson et al. (2013) and is available at the NASA Planetary Data System (PDS). The index provides a measure of the magnetospheric activity level and is calculated from magnetic field variations observed inside the magnetosphere for each orbit, normalized between 0 and 100, where 0 represents the quietest conditions and 100 the most disturbed.

Wave locations are mapped using the KT17 empirical magnetic field model (Korth et al. 2015), with field line tracing that accounts for both the MDI value and Mercury's heliocentric distance at the time of observation. This approach allows us to estimate field line connectivity and to map the wave occurrence to their magnetic footprints on Mercury's surface. Since the vast majority of the observed waves (> 97%) occur on closed field lines, only these cases are considered in the subsequent analysis to avoid mixing in other wave modes associated with open or boundary field lines.

3 Results

As noted in previous studies, ~ 1 Hz waves are a common feature of Mercury's magnetosphere. Figures 2 and 3 show statistical averages of the ~ 1 Hz wave properties over the full MESSENGER mission. Figure 2 presents the results in MSO coordinates, whereas Fig. 3 is shown in dipole magnetic coordinates using magnetic local solar time (M. LST), magnetic latitude, and L-shell (the radial distance of the field line at its magnetic equatorial crossing). The waves are predominantly observed close to the planet, within the magnetopause, with an occurrence rate of about 10–20% when normalized to the total number of magnetic field measurements made in the same regions (Figs. 2b, 3a, d). The wave power peaks in the post-midnight sector (Figs. 2d–f, 3b) although lower-amplitude waves are present throughout the closed magnetosphere. The power is dominated by the perpendicular component but shifts towards a more

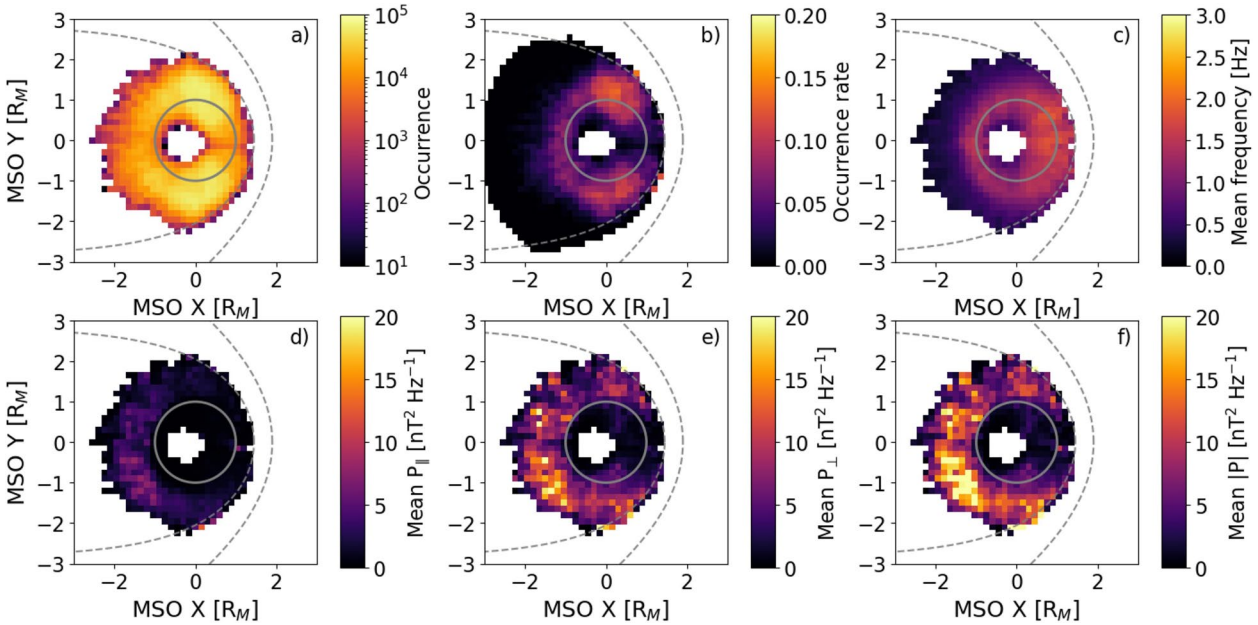

Fig. 2 Overview of ~ 1 Hz waves on closed magnetic field lines in Mercury's magnetosphere, projected onto the MSO X–Y plane. The average bow shock and magnetopause (Winslow et al. 2013) are shown as dashed grey lines, and Mercury's outline as a solid grey line. Panels show **a** total occurrence, **b** occurrence rate (ratio of wave events to total magnetic field measurements), **c** mean wave frequency, **d** mean parallel spectral power, **e** mean perpendicular spectral power, and **f** mean total spectral power. The means are calculated across all wave events within each spatial bin separately

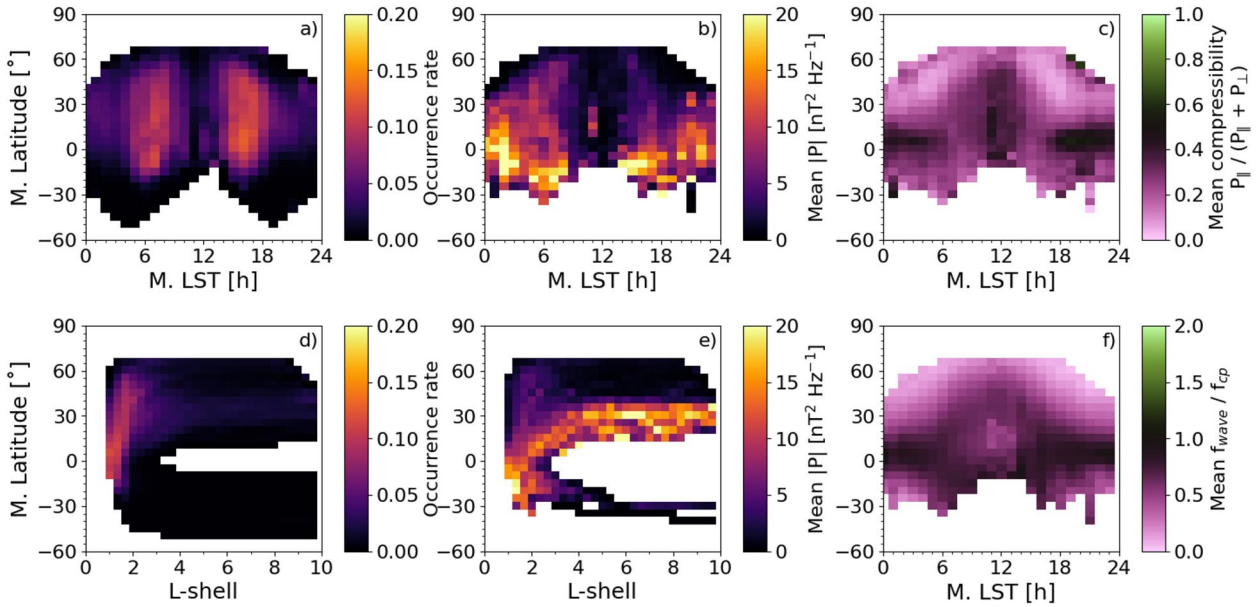

Fig. 3 Statistical overview of ~ 1 Hz waves on closed magnetic field lines in Mercury's magnetosphere. Panels **a**–**c**, **f** are shown in magnetic local solar time (M. LST) vs magnetic latitude (M. latitude), and panels **d**–**e** in magnetic latitude vs L-shell coordinates. Coordinates are given in the dipole frame centred on Mercury's magnetic dipole, offset northward by 0.196 R_M, with midnight at 0 M. LST and noon at 12 M. LST, and positive latitude northward. Panels show **a** occurrence rate, **b** mean total spectral power, **c** compressibility $P_{\parallel}/(P_{\parallel} + P_{\perp})$, **d** occurrence rate, **e** mean total spectral power, and **f** mean ratio between wave frequency and local proton cyclotron frequency (f_{wave}/f_{cp}). The means are calculated across all wave events within each spatial bin separately. It is noted that the colour bar in **c** is scaled to highlight that compressibility rarely exceeds 0.5. Similarly, the colour bar in **f** is scaled to highlight that the wave frequency never exceeds the local proton cyclotron frequency

parallel character at lower magnetic latitudes, particularly on the nightside (Figs. 2d–f, 3b, c, e). The relative variability of the total wave power within each spatial bin, computed as the standard deviation over the mean, is typically 1–2 nT^2 Hz^{-1} in the post-midnight sector and rises to ~ 5 nT^2 Hz^{-1} near the dayside flanks. This indicates a comparatively stable wave population on the nightside and a more variable distribution of wave power on the dayside. As expected, the typical wave frequencies fall in the 0.5–2 Hz range (Fig. 2c). Their frequency is close to the local proton gyrofrequency near the magnetic equator on the nightside but shift to lower values at higher magnetic latitudes, even when accounting for the stronger magnetic field there (Fig. 3f). On the dayside, by contrast, the wave frequency to local proton gyrofrequency ratio approaches unity in two off-equatorial bands displaced northward and southward of the magnetic equator (Fig. 3f), coincident with the local minimum in magnetic field strength along dayside closed field lines (not shown). The ratio decreases both towards higher magnetic latitudes and towards the dayside magnetic equator, where the local proton gyrofrequency increases.

The dataset spans March 2011–April 2015, covering almost 17 Mercury years, thereby extending the earlier statistical study of Boardsen et al. (2012), which was limited to ~ 6 months (~ 2.1 Mercury years). The results broadly agree well with those of Boardsen et al. (2012), although the present dataset does not show a clear a preference for the pre-midnight sector. This difference may be due to the much larger dataset used here, which cover a wider range of upstream conditions and period of the solar cycle. A majority of the detected waves are located on the dayside flanks, but the waves in this region have significantly lower power. Boardsen et al. (2012) applied a power threshold of 0.2 nT^2 Hz^{-1}, higher than the 0.01 nT^2 Hz^{-1} used here, which likely accounts for most of the discrepancy.

Figure 4 presents the relationship between wave occurrence and the MDI index. The occurrence rate is higher, particularly in the extended nightside, for lower MDI values. This trend cannot be explained by variations in the number of available measurements, which are relatively uniform across the four MDI intervals (Fig. 4b1–4). In contrast, the mean spectral wave power shows a strong positive correlation with increasing MDI (Fig. 4c1–4). This increase is consistent with expectations, as MDI itself reflects average wave power within the magnetosphere, and thus, the comparison primarily serves as a self-consistency check rather than providing new information. The mean compressibility (ratio of parallel to total wave power) shows no systematic variations with MDI (Fig. 4d1–4). The wave frequency scales with the local proton cyclotron frequency and increases with MDI, as expected from the associated rise in background magnetic field strength (not shown).

The orientation of the IMF also influences the occurrence of the ~ 1 Hz waves. Figure 5 shows results of the waves in the MSO X–Y plane, using intervals of the upstream IMF clock angle binned into four quadrants. Northward IMF generally produces more waves on the closed field lines than Southward, particularly for the extension in the nightside direction (Fig. 5a1–4), a trend that cannot be explained by differences in number of measurements (Fig. 5c1–4). At Mercury, the IMF is typically aligned with the Parker spiral, with cone angle ranging from 35 to 45°, depending on Mercury's orbital position due to its highly elliptical orbit around the Sun, and lying close to the MSO X–Y plane, so Northward–Southward directions are less frequently sampled (James et al. 2017), as also reflected in the number of magnetic field measurements (Fig. 5b1–4). Nevertheless, there are sufficient time periods of both Northward and Southward IMF conditions (Fig. 5b1–2) to make the results of their occurrence rate statistically significant. The wave power is generally higher for the Northward case (Fig. 5c1–2), but since much fewer waves are observed (occurrence rate is low) in the Southward case, the difference may be due to a statistical bias. Notably, Northward IMF also produces a higher occurrence rate and slightly higher wave power compared to ± Y-directed IMF, although the latter have significantly higher total number of measurements.

Figure 6 further explores the role of the IMF by examining the location of the quasi-parallel and quasi-perpendicular sides of the bow shock. Only intervals when the IMF lies near the MSO X–Y plane are included. The data are divided into cases where the IMF is approximately along the MSO Y-axis, or where the quasi-parallel bow shock is on the negative MSO Y side. The corresponding positive Y side case is excluded due to insufficient statistics. The results show that the quasi-parallel magnetosheath, despite typically higher ULF wave activity, does not lead to enhanced ~ 1 Hz wave occurrence. In fact, there is a slight decrease in occurrence inside the magnetosphere on the flank where the quasi-parallel bow shock maps onto the magnetopause. This indicates that upstream foreshock and magnetosheath waves are unlikely to be the primary generation mechanism of the ~ 1 Hz waves observed in Mercury's magnetosphere.

4 Discussion

Several key features emerge from the statistical analysis of the ~ 1 Hz waves that warrant discussion. These include the following: (1) the dependence of wave occurrence and power on the upstream IMF orientation and

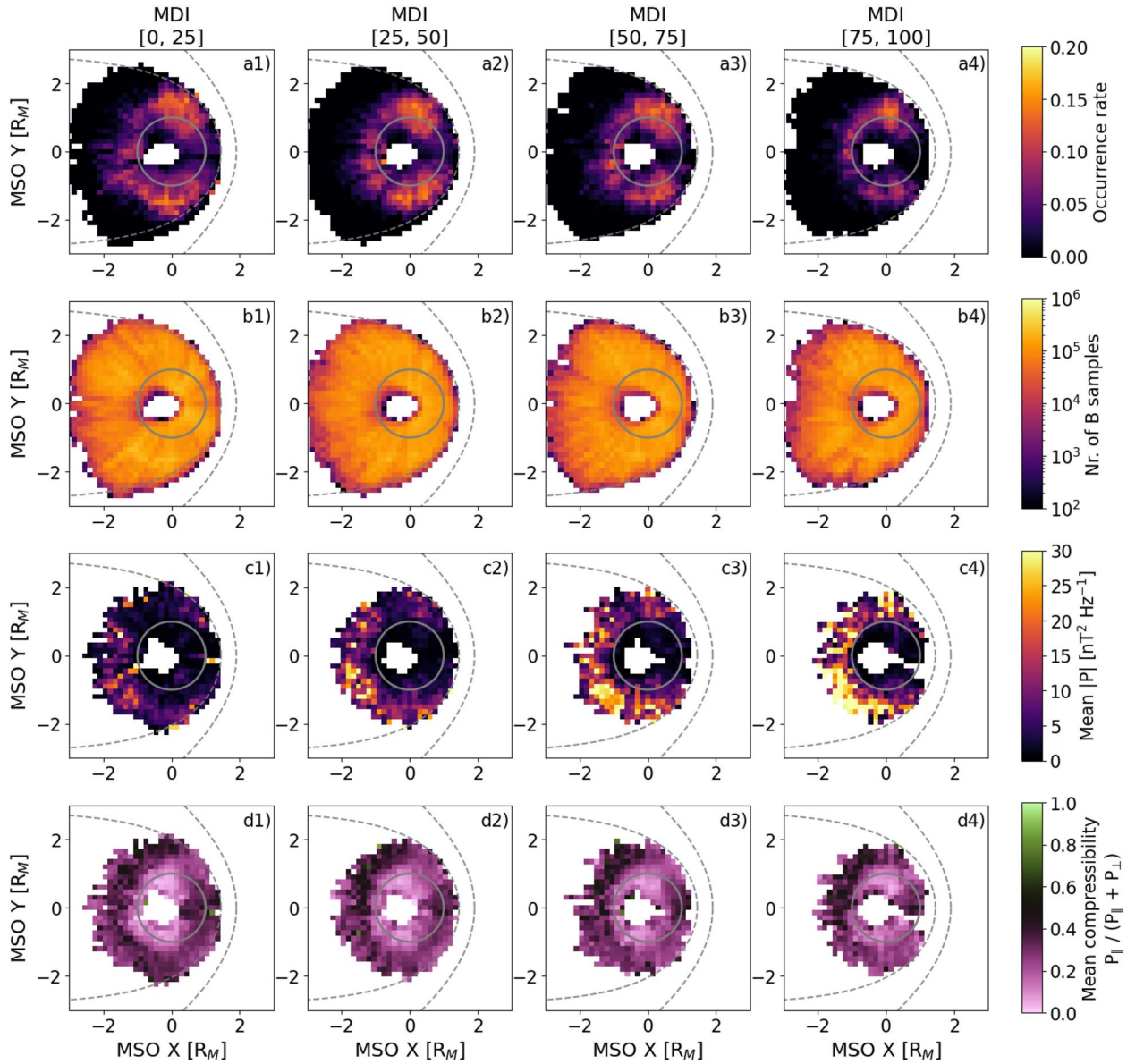

Fig. 4 Effect of magnetospheric disturbance index (MDI) on the statistical distributions of the ~ 1 Hz waves projected onto the MSO X–Y plane. The average bow shock and magnetopause (Winslow et al. 2013) are shown as dashed grey lines, and Mercury's outline as a solid grey line. The MDI for each orbit is grouped into four equal bins (0–25, 25–50, 50–75, 75–100), shown from left to right. Rows display **a** occurrence rate, **b** total number of magnetic field samples, **c** mean total wave spectral power, and **d** compressibility $P_{\parallel}/(P_{\parallel} + P_{\perp})$

on the MDI index; (2) the variation of wave frequency with magnetic latitude; and (3) the asymmetry in wave power on the nightside, with more frequent occurrence and higher amplitudes on the post-midnight (dawn) side. These features provide insight into the regions in Mercury's magnetosphere that support the ~ 1 Hz wave activity.

The occurrence of ~ 1 Hz waves is modulated by the upstream IMF and by the level of magnetospheric disturbance, as quantified by the MDI index. We note that while mean wave power correlates with MDI by construction, the occurrence of coherent ~ 1 Hz wave ridges shows the opposite trend, with enhanced occurrence at low MDI. Enhanced wave occurrence is observed during intervals of northward IMF and low MDI, i.e. when Mercury's magnetosphere is less compressed and the region of closed magnetic field lines is more extended. A northward IMF orientation increases the dayside magnetopause standoff distance and enlarges the closed field line region on the nightside, whereas a southward IMF opens many field lines and moves the

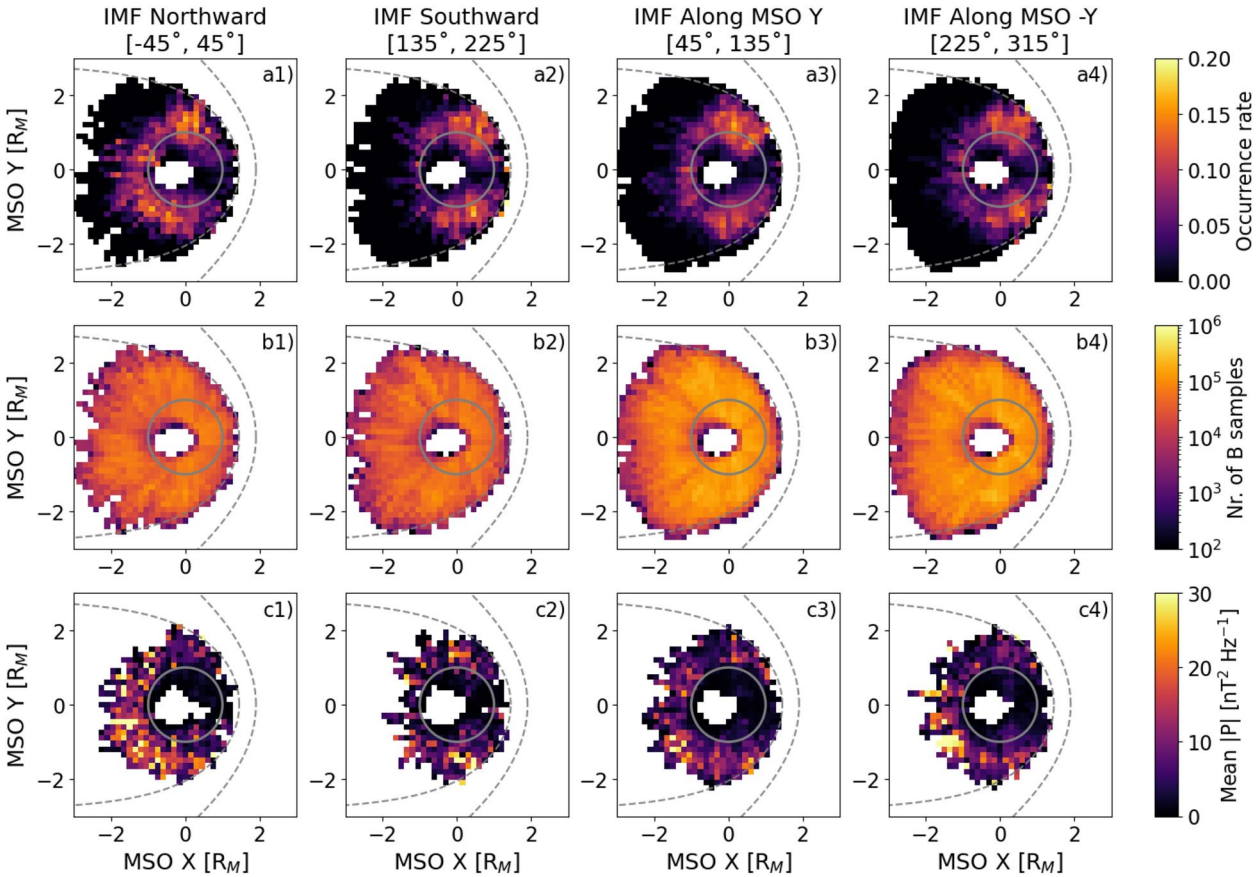

Fig. 5 Effect of IMF orientation in the MSO Y–Z plane on the statistical distributions of the ~ 1 Hz waves projected onto the MSO X–Y plane. Same structure as Fig. 4. Columns correspond to IMF directions: Northward (clock angles −45° to 45°), Southward (135°–225°), along + Y (45°–135°), and along −Y (225°–315°). Rows show **a** occurrence rate, **b** mean total wave spectral power, and **c** total number of magnetic field samples

magnetopause closer to the planet (Fatemi et al. 2020; Lavorenti et al. 2023; Slavin et al. 2019). As Southward IMF is also associated with enhanced magnetic reconnection (Slavin et al. 2021), the lower ~ 1 Hz wave occurrence under these conditions may partly reflect suppression of wave activity during active reconnection intervals. Similarly, low MDI values correspond to a more quiet magnetospheric configuration with a larger closed field region (Korth et al. 2017). The enhanced occurrence of waves under these conditions implies a strong association with closed field lines. This reinforces the view that ~ 1 Hz waves are primarily linked to plasma processes confined within Mercury's inner, quasi-stable closed field region, rather than to dynamics in the magnetosheath or open tail regions. This is further supported by the observation that upstream magnetosheath ULF wave activity, particularly present on the quasi-parallel side, does not correspond to enhanced ~ 1 Hz wave occurrence inside the magnetosphere.

While the precise wave mode of the observed ~ 1 Hz waves cannot be resolved with MESSENGER's instrumentation, their morphology, occurrence, and confinement to closed field lines allow us to make some informed speculations. Previous studies, consistent with our observations, show that these waves typically have frequencies just below the proton gyrofrequency f_{cp}, wave vector $\vec{k}$ mostly perpendicular to the magnetic field, and clear electromagnetic signatures in the magnetic field (B_{wave}). On the nightside, the observed wave frequencies are typically close to the local proton gyrofrequency near the magnetic equator but decrease relative to f_{cp} at higher latitudes. On the dayside, the frequencies remain close to the local proton gyrofrequency in two off-equatorial bands. This behaviour is naturally explained if the waves are generated near the local minimum magnetic field strength region along closed field lines, similar to EMIC waves observed at Earth (Allen et al. 2015). On the dayside, this minimum occurs off the magnetic equator, while on the nightside it lies close to the equator, in agreement with the observed latitudinal structure (Fig. 3f). In this interpretation, the waves propagate

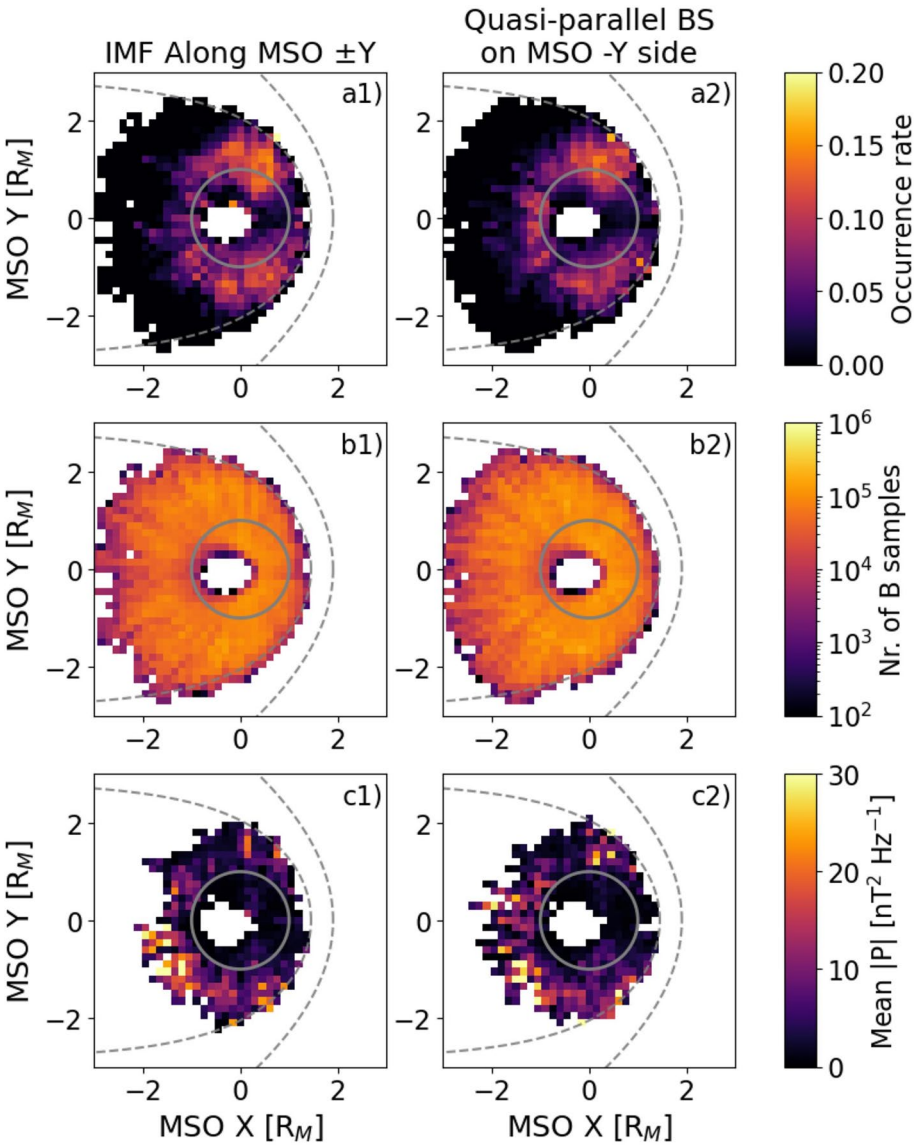

Fig. 6 Effect of IMF orientation with respect to the bow shock on the statistical distributions of the ~ 1 Hz waves projected onto the MSO X–Y plane. Same structure as Fig. 5. Only intervals with the IMF close to the MSO X–Y plane are included. Columns correspond to conditions where the IMF is approximately along MSO ±Y (left) or produce a quasi-parallel bow shock on the –Y side (right) as illustrated by the black arrows in panels **a1**, **2**. The case with a quasi-parallel bow shock on the +Y side is excluded due to insufficient statistics

along the closed field lines with an approximately constant intrinsic frequency. As magnetic field strength increases with latitude, the local proton gyrofrequency rises, reducing the ratio of observed frequency to proton gyrofrequency. While a Doppler shift due to spacecraft motion or bulk plasma convection cannot be fully excluded to explain the relative lowering of the frequency (Boardsen et al. 2015), the systematic and hemispherically symmetric latitude dependence strongly supports field-aligned propagation from a near-minimum magnetic field strength source region.

Waves with these characteristics are often classified as EMIC waves, a left-hand polarized mode propagating below the proton gyrofrequency, which in the hydromagnetic limit is typically referred to as Alfvén waves (André, 1985). Their wave vectors may range from parallel to nearly perpendicular to the magnetic field, and in our observations the perpendicular component dominates. EMIC waves can be generated by temperature anisotropies ($T_\perp/T_\parallel > 1$), loss-cone distributions, or particle beams. Loss-cone distributions have indeed been observed on Mercury's closed field lines (Boardsen et al.

2015; Zhao et al. 2022a). Additionally, upper harmonics (i.e. frequencies near integer multiples of the proton cyclotron frequency) have been observed in connection with the ~ 1 Hz waves, particularly near the magnetic equator (Boardsen et al. 2012). These harmonics have been suggested to correspond to so-called electromagnetic ion Bernstein-type waves (Boardsen et al. 2015). In the simplest case, when the wave vector is strictly perpendicular to the magnetic field, these harmonics are electrostatic. However, a finite parallel component generates a measurable magnetic field signature (André 1985), making them observable by MESSENGER. A detailed study of these observed harmonic structures is an interesting direction for future research. In particular, future observations by BepiColombo's electric field instrument could reveal a larger occurrence rate of the waves, including cases where they are predominantly electrostatic and thus not detectable by MESSENGER.

Even without identifying the precise wave mode, the observed preference of the ~ 1 Hz waves for closed magnetic field lines does suggest a link to semi-trapped particle populations (Zhao et al. 2022a). Such populations can produce loss-cone distributions, which could supply the free energy necessary for wave generation. The resulting waves, typically associated with ion Bernstein or EMIC wave modes (Boardsen et al. 2015), can in turn scatter particles into the loss cone, leading to precipitation and contributing to the gradual decay of the partial ring current. This is consistent with the quasi-trapped nature of Mercury's closed field ion populations, which often do not complete full drift orbits before impacting the surface or escaping the magnetosphere (Schriver et al. 2011; Trávníček et al. 2010; Zhao et al. 2022a). The similarity between the ~ 1 Hz wave distribution and the global morphology of the partial ring current (Zhao et al. 2022a) supports this interpretation.

However, this mechanism requires a continual replenishment of energetic particles, which may explain why ~ 1 Hz waves are not observed continuously on closed field lines. Such replenishment can be provided by frequent tail reconnection and flux transfer event (FTE) trains, which operate on short timescales and can periodically inject energetic plasma onto closed field lines (Imber et al. 2014; Slavin et al. 2012; Zhong et al. 2018). In this sense, the ~ 1 Hz waves are linked to the Dungey cycle but are not directly driven by reconnection itself.

The indirect link between reconnection-driven particle injections and the ~ 1 Hz wave occurrence also explains the observed post-midnight asymmetry in nightside wave power. Magnetospheric drift flow patterns arising from the combined action of the E × B, gradient, and curvature drifts produce enhanced dawnward proton transport (Korth et al. 2011a). This generates asymmetries in observed plasma characteristics at Mercury: enhanced plasma density and proton fluxes on the dawn side (Korth et al. 2014), a plasma sheet displaced towards dawn (Boardsen et al. 2015; Korth et al. 2011a), and dipolarizations and plasma outflows from reconnection events preferentially occurring in the post-midnight sector (Baker et al. 2016; Dewey et al. 2017; Slavin et al. 2021). These plasma asymmetries provide favourable conditions for the generation of the ~ 1 Hz waves on post-midnight closed field lines, causing their wave power to peak in this region. This interpretation is further supported by local observations showing that periodic modulations of proton fluxes are reflected in the wave power of the ~ 1 Hz waves (Zhao et al. 2022b), although future studies should aim to directly characterize the relationship between the ~ 1 Hz waves and the particle distributions on closed field lines to further test the proposed wave–particle coupling and energy transport mechanisms.

While this study provides new statistical insight into the ~ 1 Hz waves within Mercury's magnetosphere, several limitations arise from the assumptions used for both the upstream conditions and the magnetic field model. First, the KT17 model accounts only for the MDI index and Mercury's heliocentric distance, but not for the IMF direction or other upstream parameters that may alter the magnetospheric configuration. Consequently, field line mapping from the point of observation may be biased under certain solar wind conditions. Nevertheless, the KT17 model is empirically derived from MESSENGER observations and generally reproduces the local magnetic field measurements with small residuals (Korth et al. 2017).

Second, the upstream solar wind and IMF conditions were determined from intervals when MESSENGER was located outside the bow shock, which could be up to an hour separated in time from the wave observations made within the closed field line region. Large-scale magnetospheric dynamics at Mercury evolve on shorter timescales (Slavin et al. 2021), so temporal variations in the upstream conditions could influence the correlation analysis. The IMF typically remains in a similar orientation for about 20 min at Mercury's orbit (James et al. 2017), implying that changes between the upstream and internal measurements may occasionally occur. However, the statistical significance of the dataset, covering more than 4000 orbits, should largely mitigate these effects when averaged over many events.

Another limitation is the inclusion of intervals affected by large-scale space weather phenomena such as interplanetary coronal mass ejections (ICMEs). These have not been explicitly excluded and could introduce variability in both the closed magnetic field configuration and the generation of waves. A targeted future study focusing

on ICME intervals could help disentangle their influence on the occurrence and characteristics of these ~ 1 Hz waves. Finally, MESSENGER's orbital geometry limits the ability to clearly separate seasonal and latitudinal effects, since the spacecraft's orbital plane was strongly biased towards specific local times and seasons.

5 BepiColombo perspectives

The upcoming BepiColombo mission (Benkhoff et al. 2021; Murakami et al. 2020) will overcome many of the limitations of MESSENGER and provide a major step forward in understanding the physical nature of the ~ 1 Hz waves. BepiColombo consists of two spacecraft: the Mercury Magnetospheric Orbiter (MMO, now Mio) and the Mercury Planetary Orbiter (MPO), with nearly polar and complementary orbits (Fig. 7). Mio and MPO have nominal pericentres of 590 km and 480 km, respectively, and their orbits precess with Mercury's orbital motion around the Sun, enabling near-complete coverage of local time sectors and magnetic latitudes, and at times allowing simultaneous sampling of open and closed field line regions. This geometry will allow detailed studies of both dawn–dusk and north–south asymmetries, the latter being particularly important given the northward offset of Mercury's intrinsic magnetic dipole.

BepiColombo's instrumentation offers further advantages. Mio carries a comprehensive plasma suite, including AC–DC electric and magnetic field sensors (Baumjohann et al. 2020; Karlsson et al. 2020; Kasaba et al. 2020) and full-sky ion/electron spectrometers enabled by the spacecraft's 4 s spin (Saito et al. 2021). These measurements will allow us to better constrain the plasma environment and the waves, provide Poynting flux, and examine wave growth conditions. MPO complements these measurements with a magnetometer (Heyner et al. 2021) and additional plasma instruments (Orsini et al. 2021). The two-spacecraft configuration enables simultaneous measurements linking upstream solar wind and IMF conditions to plasma and wave dynamics within the magnetosphere. For example, while Mio traverses the post-midnight closed field line region, MPO may be located upstream in the magnetosheath, serving as a proxy for the upstream solar wind (Bowers et al. 2024; Gershman et al. 2012). In other configurations, the dual magnetometers will allow direct observations of the waves at two points, constraining their propagation and spatial structure (Baumjohann et al. 2020; Heyner et al. 2021).

Overall, the MESSENGER results provide the first global context for these ~ 1 Hz waves, indicating that they occur predominantly on closed field lines and are controlled by upstream conditions and magnetospheric topology. BepiColombo's dual-spacecraft measurements will allow these interpretations to be tested directly, linking wave properties to plasma distributions, Poynting flux, magnetic topology, and upstream variability.

6 Conclusions

In this study, we investigated the location and characteristics of the previously reported ~ 1 Hz waves in Mercury's magnetosphere, using the full set of magnetometer measurements from MESSENGER. We find that these waves predominantly occur on closed magnetic field lines, with an overall occurrence rate of about 10–20%. Their region of occurrence expands under conditions when the closed field line region itself extends, highlighting a dependence on upstream and magnetospheric conditions. The region of maximum wave power is located in the post-midnight sector near the magnetic equator. The observed frequencies

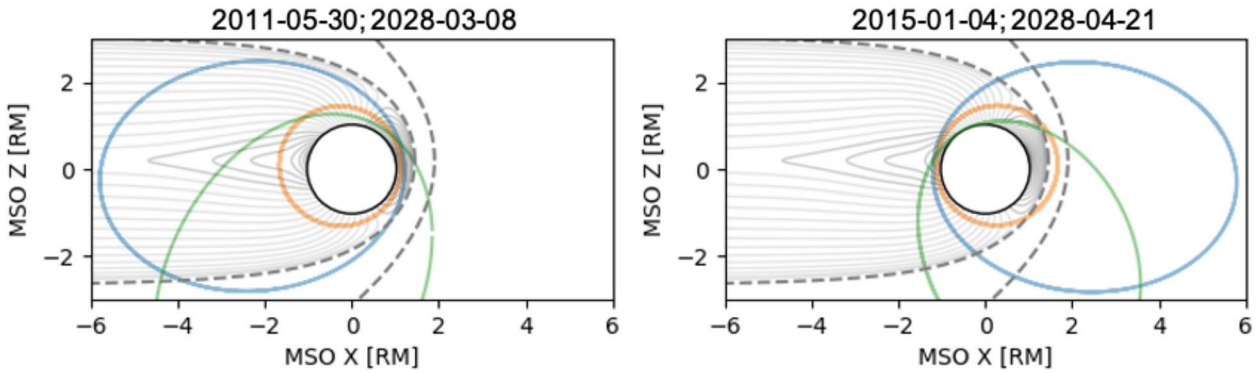

Fig. 7 Planned orbits of the two BepiColombo spacecraft: the Mercury Magnetospheric Orbiter (Mio, blue) and the Mercury Planetary Orbiter (MPO, orange), projected onto the MSO X–Z plane at two dates separated by half a Mercury year to illustrate orbital precession. Two sample MESSENGER orbits (green) are shown for comparison. Dashed grey lines indicate the average locations of the magnetopause and bow shock, while faint grey lines show the average KT17 model magnetic field lines at a heliocentric distance of 0.39 AU and MDI = 50

are close to the local proton cyclotron frequency at the equator on the nightside, and in two off-equatorial bands on the dayside, decreasing towards sub-cyclotron values both at higher magnetic latitudes and towards the dayside magnetic equator, where the local field strength is enhanced along closed field lines.

We interpret the ~ 1 Hz waves as being generated near the magnetic equator, likely associated with semi-trapped particle populations and the loss-cone distributions inferred from previous studies, which are periodically replenished by reconnection-driven injections from the tail plasma sheet. These waves are thus likely linked indirectly to the Dungey cycle and shaped by magnetospheric drift flow patterns, producing the observed post-midnight asymmetries in wave occurrence and power. Future studies should aim to further clarify the connection between the ~ 1 Hz waves and particle distributions. These results indicate that the ~ 1 Hz waves may play an active role in shaping Mercury's inner magnetospheric dynamics and serve as an important diagnostic of magnetospheric processes.

The upcoming BepiColombo mission, arriving at Mercury in late 2026, will provide crucial new observations to test these interpretations. Its dual-spacecraft configuration will allow simultaneous measurements of upstream conditions and inner magnetospheric responses, complementing the statistical context established by MESSENGER. Together, these observations will enable a comprehensive understanding of the generation, propagation, and role of ~ 1 Hz waves in Mercury's plasma environment.

Acknowledgements
The authors acknowledge all members of the MESSENGER mission, in particular the magnetometer team, for their contributions to the success of the mission.

Author contributions
M.P. designed the study, performed the analysis, and wrote the manuscript. A.D. contributed to the refinement of the analysis methods and to the scientific interpretation of the results. J.W.E. and M.M. contributed to the interpretation and discussion of the results. A.E. and M.A. provided input on the wave mode discussion. E.Y., L.H., S.A., Y.K., and N.E. contributed to discussions and reviewed the manuscript. All authors read and approved the final version of the manuscript.

Funding
Open access funding provided by Uppsala University. M.P. and E.Y. gratefully acknowledge support from the Swedish National Space Agency under Grants Dnr 2023-00183 (M.P.) and Dnr 2024-0209 (E.Y.).

Data availability
The high-resolution magnetic field data from the MESSENGER fluxgate magnetometer (https://doi.org/10.17189/1522385) and the MESSENGER disturbance index (MDI; Anderson et al. 2013) used in this study are publicly available via the NASA Planetary Data System (https://pds-ppi.igpp.ucla.edu/mission/MESSENGER). The bow shock crossings database is taken from Sun (2023).

Declarations

Competing interests
The authors declare no competing interests.

Author details
[1]Swedish Institute of Space Physics, Uppsala, Sweden. [2]LPP, CNRS, École Polytechnique, Institut Polytechnique de Paris, Observatoire de Paris, Sorbonne Université, Université Paris Saclay, Palaiseau, France.

Received: 22 November 2025 Accepted: 29 July 2026
Published online: 14 August 2026

References

Alexeev II, Belenkaya ES, Slavin JA, Korth H, Anderson BJ, Baker DN, Boardsen SA, Johnson CL, Purucker ME, Sarantos M, Solomon SC (2010) Mercury's magnetospheric magnetic field after the first two MESSENGER flybys. Icarus 209:23–39. https://doi.org/10.1016/j.icarus.2010.01.024

Allen RC, Zhang J-C, Kistler LM, Spence HE, Lin R-L, Klecker B, Dunlop MW, André M, Jordanova VK (2015) A statistical study of EMIC waves observed by Cluster: 1. Wave properties. J Geophys Res Space Phys 120:5574–5592. https://doi.org/10.1002/2015JA021333

Anderson BJ, Acuna MH, Lohr DA, Scheifele J, Raval A, Korth H, Slavin JA (2007) The magnetometer instrument on MESSENGER. In: Domingue DL, Russell CT (eds) The messenger mission to Mercury. Springer, New York, pp 417–450. https://doi.org/10.1007/978-0-387-77214-1_12

Anderson BJ, Acuña MH, Korth H, Slavin JA, Uno H, Johnson CL, Purucker ME, Solomon SC, Raines JM, Zurbuchen TH, Gloeckler G, McNutt RL (2010) The magnetic field of Mercury. Space Sci Rev 152:307–339. https://doi.org/10.1007/s11214-009-9544-3

Anderson BJ, Johnson CL, Korth H, Winslow RM, Borovsky JE, Purucker ME, Slavin JA, Solomon SC, Zuber MT, McNutt RL Jr. (2012) Low-degree structure in Mercury's planetary magnetic field. J Geophys Res Planets. https://doi.org/10.1029/2012JE004159

Anderson BJ, Johnson CL, Korth H (2013) A magnetic disturbance index for Mercury's magnetic field derived from MESSENGER magnetometer data. Geochem Geophys Geosyst 14:3875–3886. https://doi.org/10.1002/ggge.20242

André M (1985) Dispersion surfaces. J Plasma Phys 33:1–19. https://doi.org/10.1017/S0022377800002270

Baker DN, Dewey RM, Lawrence DJ, Goldsten JO, Peplowski PN, Korth H, Slavin JA, Krimigis SM, Anderson BJ, Ho GC, McNutt RL, Raines JM, Schriver D, Solomon SC (2016) Intense energetic electron flux enhancements in Mercury's magnetosphere: an integrated view with high-resolution observations from MESSENGER. J Geophys Res Space Phys 121:2171–2184. https://doi.org/10.1002/2015JA021778

Baumjohann W, Matsuoka A, Narita Y, Magnes W, Heyner D, Glassmeier K-H, Nakamura R, Fischer D, Plaschke F, Volwerk M, Zhang TL, Auster H-U, Richter I, Balogh A, Carr CM, Dougherty M, Horbury TS, Tsunakawa H, Matsushima M, Shinohara M, Shibuya H, Nakagawa T, Hoshino M, Tanaka Y, Anderson BJ, Russell CT, Motschmann U, Takahashi F, Fujimoto A (2020) The BepiColombo–Mio magnetometer en route to Mercury. Space Sci Rev 216:125. https://doi.org/10.1007/s11214-020-00754-y

Benkhoff J, Murakami G, Baumjohann W, Besse S, Bunce E, Casale M, Cremosese G, Glassmeier K-H, Hayakawa H, Heyner D, Hiesinger H, Huovelin J, Hussmann H, Iafolla V, Iess L, Kasaba Y, Kobayashi M, Milillo A, Mitrofanov IG, Montagnon E, Novara M, Orsini S, Quemerais E, Reininghaus U, Saito Y, Santoli F, Stramaccioni D, Sutherland O, Thomas N, Yoshikawa I, Zender J (2021) BepiColombo—Mission overview and science goals. Space Sci Rev 217:90. https://doi.org/10.1007/s11214-021-00861-4

Boardsen SA, Slavin JA, Anderson BJ, Korth H, Solomon SC (2009) Comparison of ultra-low-frequency waves at Mercury under northward and southward IMF. Geophys Res Lett. https://doi.org/10.1029/2009GL039525

Boardsen SA, Slavin JA, Anderson BJ, Korth H, Schriver D, Solomon SC (2012) Survey of coherent ~1 Hz waves in Mercury's inner magnetosphere from MESSENGER observations. J Geophys Res Space Phys. https://doi.org/10.1029/2012JA017822

Boardsen SA, Kim E-H, Raines JM, Slavin JA, Gershman DJ, Anderson BJ, Korth H, Sundberg T, Schriver D, Travnicek P (2015) Interpreting 1 Hz magnetic compressional waves in Mercury's inner magnetosphere in terms of propagating ion-Bernstein waves. J Geophys Res Space Phys 120:4213–4228. https://doi.org/10.1002/2014JA020910

Bowers CF, Jackman CM, Azari AR, Smith AW, Wright PJ, Rutala MJ, Sun W, Healy A (2024) Estimating interplanetary magnetic field conditions at Mercury's orbit from MESSENGER magnetosheath observations using a feedforward neural network. J Geophys Res Mach Learn Comput 1:e2024JH000239. https://doi.org/10.1029/2024JH000239

Cowley SWH (1981) Magnetospheric asymmetries associated with the y-component of the IMF. Planet Space Sci 29:79–96. https://doi.org/10.1016/0032-0633(81)90141-0

Dewey RM, Slavin JA, Raines JM, Baker DN, Lawrence DJ (2017) Energetic electron acceleration and injection during dipolarization events in Mercury's magnetotail. J Geophys Res Space Phys 122:12170–12188. https://doi.org/10.1002/2017JA024617

DiBraccio GA, Slavin JA, Boardsen SA, Anderson BJ, Korth H, Zurbuchen TH, Raines JM, Baker DN, McNutt RL Jr., Solomon SC (2013) MESSENGER observations of magnetopause structure and dynamics at Mercury. J Geophys Res Space Phys 118:997–1008. https://doi.org/10.1002/jgra.50123

Fatemi S, Poppe AR, Barabash S (2020) Hybrid simulations of solar wind proton precipitation to the surface of Mercury. J Geophys Res Space Phys 125:e2019JA027706. https://doi.org/10.1029/2019JA027706

Gershman DJ, Zurbuchen TH, Fisk LA, Gilbert JA, Raines JM, Anderson BJ, Smith CW, Korth H, Solomon SC (2012) Solar wind alpha particles and heavy ions in the inner heliosphere observed with MESSENGER. J Geophys Res Space Phys. https://doi.org/10.1029/2012JA017829

Heyner D, Auster H-U, Fornaçon K-H, Carr C, Richter I, Mieth JZD, Kolhey P, Exner W, Motschmann U, Baumjohann W, Matsuoka A, Magnes W, Berghofer G, Fischer D, Plaschke F, Nakamura R, Narita Y, Delva M, Volwerk M, Balogh A, Dougherty M, Horbury T, Langlais B, Mandea M, Masters A, Oliveira JS, Sánchez-Cano B, Slavin JA, Vennerstrøm S, Vogt J, Wicht J, Glassmeier K-H (2021) The BepiColombo planetary magnetometer MPO-MAG: what can we learn from the Hermean magnetic field? Space Sci Rev 217:52. https://doi.org/10.1007/s11214-021-00822-x

Imber SM, Slavin JA (2017) MESSENGER observations of magnetotail loading and unloading: implications for substorms at Mercury. J Geophys Res Space Phys 122:11402–11412. https://doi.org/10.1002/2017JA024332

Imber SM, Slavin JA, Boardsen SA, Anderson BJ, Korth H, McNutt RL Jr., Solomon SC (2014) MESSENGER observations of large dayside flux transfer events: do they drive Mercury's substorm cycle? J Geophys Res Space Phys 119:5613–5623. https://doi.org/10.1002/2014JA019884

James MK, Bunce EJ, Yeoman TK, Imber SM, Korth H (2016) A statistical survey of ultralow-frequency wave power and polarization in the Hermean magnetosphere. J Geophys Res Space Phys 121:8755–8772. https://doi.org/10.1002/2016JA023103

James MK, Imber SM, Bunce EJ, Yeoman TK, Lockwood M, Owens MJ, Slavin JA (2017) Interplanetary magnetic field properties and variability near Mercury's orbit. J Geophys Res Space Phys 122:7907–7924. https://doi.org/10.1002/2017JA024435

Jarvinen R, Alho M, Kallio E, Pulkkinen TI (2020) Ultra-low-frequency waves in the ion foreshock of Mercury: a global hybrid modelling study. Mon Not R Astron Soc 491:4147–4161. https://doi.org/10.1093/mnras/stz3257

Jia X, Slavin JA, Poh G, DiBraccio GA, Toth G, Chen Y, Raines JM, Gombosi TI (2019) MESSENGER observations and global simulations of highly compressed magnetosphere events at Mercury. J Geophys Res Space Phys 124:229–247. https://doi.org/10.1029/2018JA026166

Kallio E, Jarvinen R, Massetti S, Alberti T, Milillo A, Orsini S, De Angelis E, Laky G, Slavin J, Raines JM, Pulkkinen TI (2022) Ultra-low frequency waves in the Hermean magnetosphere: on the role of the morphology of the magnetic field and the foreshock. Geophys Res Lett 49:e2022GL101850. https://doi.org/10.1029/2022GL101850

Karlsson T, Kasaba Y, Wahlund J-E, Henri P, Bylander L, Puccio W, Jansson S-E, Åhlen L, Kallio E, Kojima H, Kumamoto A, Lappalainen K, Lybekk B, Ishisaka K, Eriksson A, Morooka M (2020) The MEFISTO and WPT electric field sensors of the plasma wave investigation on the BepiColombo Mio spacecraft. Space Sci Rev 216:132. https://doi.org/10.1007/s11214-020-00760-0

Kasaba Y, Kojima H, Moncuquet M, Wahlund J-E, Yagitani S, Sahraoui F, Henri P, Karlsson T, Kasahara Y, Kumamoto A, Ishisaka K, Issautier K, Wattieaux G, Imachi T, Matsuda S, Lichtenberger J, Usui H (2020) Plasma wave investigation (PWI) aboard BepiColombo Mio on the trip to the first measurement of electric fields, electromagnetic waves, and radio waves around Mercury. Space Sci Rev 216:65. https://doi.org/10.1007/s11214-020-00692-9

Korth H, Anderson BJ, Raines JM, Slavin JA, Zurbuchen TH, Johnson CL, Purucker ME, Winslow RM, Solomon SC, McNutt RL (2011a) Plasma pressure in Mercury's equatorial magnetosphere derived from MESSENGER Magnetometer observations. Geophys Res Lett. https://doi.org/10.1029/2011GL049451

Korth H, Anderson BJ, Zurbuchen TH, Slavin JA, Perri S, Boardsen SA, Baker DN, Solomon SC, McNutt RL (2011b) The interplanetary magnetic field environment at Mercury's orbit. Planet Space Sci 59:2075–2085. https://doi.org/10.1016/j.pss.2010.10.014

Korth H, Anderson BJ, Gershman DJ, Raines JM, Slavin JA, Zurbuchen TH, Solomon SC, McNutt RL Jr (2014) Plasma distribution in Mercury's magnetosphere derived from MESSENGER magnetometer and fast imaging plasma spectrometer observations. J Geophys Res Space Phys 119:2917–2932. https://doi.org/10.1002/2013JA019567

Korth H, Tsyganenko NA, Johnson CL, Philpott LC, Anderson BJ, Al Asad MM, Solomon SC, McNutt RL Jr (2015) Modular model for Mercury's magnetospheric magnetic field confined within the average observed magnetopause. J Geophys Res Space Phys 120:4503–4518. https://doi.org/10.1002/2015JA021022

Korth H, Johnson CL, Philpott L, Tsyganenko NA, Anderson BJ (2017) A dynamic model of Mercury's magnetospheric magnetic field. Geophys Res Lett 44:10,147-10,154. https://doi.org/10.1002/2017GL074699

Lavorenti F, Jensen EA, Aizawa S, Califano F, D'Amore M, Domingue D, Henri P, Lindsay S, Raines JM, Savin DW (2023) Maps of solar wind plasma precipitation onto Mercury's surface: a geographical perspective. Planet Sci J 4:163. https://doi.org/10.3847/PSJ/acef15

Li R, Sun W, Fu S, Dewey RM, Zhao J, Jackman CM, Slavin JA, Poh GK, Raines JM, Lu S, Guo J, Luo Z, Pu Z, Xie L (2025) Observations of Kelvin-Helmholtz waves on Mercury's pre-dawnside magnetopause: MESSENGER case study. J Geophys Res Space Phys 130:e2025JA033828. https://doi.org/10.1029/2025JA033828

Liljeblad E, Karlsson T (2017) Investigation of ∼ 20–40 mHz ULF waves and their driving mechanisms in Mercury's dayside magnetosphere. Ann Geophys 35:879–884. https://doi.org/10.5194/angeo-35-879-2017

Liljeblad E, Sundberg T, Karlsson T, Kullen A (2014) Statistical investigation of Kelvin-Helmholtz waves at the magnetopause of Mercury. J Geophys Res Space Phys 119:9670–9683. https://doi.org/10.1002/2014JA020614

Liljeblad E, Karlsson T, Sundberg T, Kullen A (2016) Observations of magnetospheric ULF waves in connection with the Kelvin-Helmholtz instability at Mercury. J Geophys Res Space Phys 121:8576–8588. https://doi.org/10.1002/2016JA023015

Lockwood M, Owens MJ, Imber SM, James MK, Bunce EJ, Yeoman TK (2017) Coronal and heliospheric magnetic flux circulation and its relation to open solar flux evolution. J Geophys Res Space Phys 122:5870–5894. https://doi.org/10.1002/2016JA023644

Means JD (1972) Use of the three-dimensional covariance matrix in analyzing the polarization properties of plane waves. J Geophys Res 77:5551–5559. https://doi.org/10.1029/JA077i028p05551

Murakami G, Hayakawa H, Ogawa H, Matsuda S, Seki T, Kasaba Y, Saito Y, Yoshikawa I, Kobayashi M, Baumjohann W, Matsuoka A, Kojima H, Yagitani S, Moncuquet M, Wahlund J-E, Delcourt D, Hirahara M, Barabash S, Korablev O, Fujimoto M (2020) Mio—first comprehensive exploration of Mercury's space environment: mission overview. Space Sci Rev 216:113. https://doi.org/10.1007/s11214-020-00733-3

Orsini S, Livi SA, Lichtenegger H, Barabash S, Milillo A, De Angelis E, Phillips M, Laky G, Wieser M, Olivieri A, Plainaki C, Ho G, Killen RM, Slavin JA, Wurz P, Berthelier J-J, Dandouras I, Kallio E, McKenna-Lawlor S, Szalai S, Torkar K, Vaisberg O, Allegrini F, Daglis IA, Dong C, Escoubet CP, Fatemi S, Fränz M, Ivanovski S, Krupp N, Lammer H, Leblanc F, Mangano V, Mura A, Nilsson H, Raines JM, Rispoli R, Sarantos M, Smith HT, Szego K, Aronica A, Camozzi F, Di Lellis AM, Fremuth G, Giner F, Gurnee R, Hayes J, Jeszenszky H, Tominetti F, Trantham B, Balaz J, Baumjohann W, Brienza D, Bührke U, Bush MD, Cantatore M, Cibella S, Colasanti L, Cremonese G, Cremonesi L, D'Alessandro M, Delcourt D, Delva M, Desai M, Fama M, Ferris M, Fischer

H, Gaggero A, Gamborino D, Garnier P, Gibson WC, Goldstein R, Grande M, Grishin V, Haggerty D, Holmström M, Horvath I, Hsieh K-C, Jacques A, Johnson RE, Kazakov A, Kecskemety K, Krüger H, Kürbisch C, Lazzarotto F, Leblanc F, Leichtfried M, Leoni R, Loose A, Maschietti D, Massetti S, Mattioli F, Miller G, Moissenko D, Morbidini A, Noschese R, Nuccilli F, Nunez C, Paschalidis N, Persyn S, Piazza D, Oja M, Ryno J, Schmidt W, Scheer JA, Shestakov A, Shuvalov S, Seki K, Selci S, Smith K, Sordini R, Svensson J, Szalai L, Toublanc D, Urdiales C, Varsani A, Vertolli N, Wallner R, Wahlstroem P, Wilson P, Zampieri S (2021) SERENA: particle instrument suite for determining the Sun-Mercury interaction from BepiColombo. Space Sci Rev 217:11. https://doi.org/10.1007/s11214-020-00787-3

Raines JM, Gershman DJ, Zurbuchen TH, Sarantos M, Slavin JA, Gilbert JA, Korth H, Anderson BJ, Gloeckler G, Krimigis SM, Baker DN, McNutt RL Jr., Solomon SC (2013) Distribution and compositional variations of plasma ions in Mercury's space environment: the first three Mercury years of MESSENGER observations. J Geophys Res Space Phys 118:1604–1619. https://doi.org/10.1029/2012JA018073

Romanelli N, DiBraccio G, Gershman D, Le G, Mazelle C, Meziane K, Boardsen S, Slavin J, Raines J, Glass A, Espley J (2020) Upstream ultra-low frequency waves observed by MESSENGER's magnetometer: implications for particle acceleration at Mercury's bow shock. Geophys Res Lett 47:e2020GL087350. https://doi.org/10.1029/2020GL087350

Saito Y, Delcourt D, Hirahara M, Barabash S, André N, Takashima T, Asamura K, Yokota S, Wieser M, Nishino MN, Oka M, Futaana Y, Harada Y, Sauvaud J-A, Louarn P, Lavraud B, Génot V, Mazelle C, Dandouras I, Jacquey C, Aoustin C, Barthe A, Cadu A, Fedorov A, Frezoul A-M, Garat C, Le Comte E, Lee Q-M, Médale J-L, Moirin D, Penou E, Petiot M, Peyre G, Rouzaud J, Séran H-C, Němeček Z, Šafránková J, Marcucci MF, Bruno R, Consolini G, Miyake W, Shinohara I, Hasegawa H, Seki K, Coates AJ, Leblanc F, Verdeil C, Katra B, Fontaine D, Illiano J-M, Berthelier J-J, Techer J-D, Fraenz M, Fischer H, Krupp N, Woch J, Bührke U, Fiethe B, Michalik H, Matsumoto H, Yanagimachi T, Miyoshi Y, Mitani T, Shimoyama M, Zong Q, Wurz P, Andersson H, Karlsson S, Holmström M, Kazama Y, Ip W-H, Hoshino M, Fujimoto M, Terada N, Keika K, BepiColombo Mio/MPPE Team (2021) Pre-flight calibration and near-Earth commissioning results of the Mercury Plasma Particle Experiment (MPPE) onboard MMO (Mio). Space Sci Rev 217:70. https://doi.org/10.1007/s11214-021-00839-2

Schmid D, Narita Y, Plaschke F, Volwerk M, Nakamura R, Baumjohann W (2021) Pick-up ion cyclotron waves around Mercury. Geophys Res Lett 48:e2021GL092606. https://doi.org/10.1029/2021GL092606

Schriver D, Trávníček PM, Anderson BJ, Ashour-Abdalla M, Baker DN, Benna M, Boardsen SA, Gold RE, Hellinger P, Ho GC, Korth H, Krimigis SM, McNutt RL Jr, Raines JM, Richard RL, Slavin JA, Solomon SC, Starr RD, Zurbuchen TH (2011) Quasi-trapped ion and electron populations at Mercury. Geophys Res Lett. https://doi.org/10.1029/2011GL049629

Slavin JA, Anderson BJ, Baker DN, Benna M, Boardsen SA, Gloeckler G, Gold RE, Ho GC, Korth H, Krimigis SM, McNutt RL, Nittler LR, Raines JM, Sarantos M, Schriver D, Solomon SC, Starr RD, Trávníček PM, Zurbuchen TH (2010) MESSENGER observations of extreme loading and unloading of Mercury's magnetic tail. Science 329:665–668. https://doi.org/10.1126/science.1188067

Slavin JA, Imber SM, Boardsen SA, DiBraccio GA, Sundberg T, Sarantos M, Nieves-Chinchilla T, Szabo A, Anderson BJ, Korth H, Zurbuchen TH, Raines JM, Johnson CL, Winslow RM, Killen RM, McNutt RL Jr, Solomon SC (2012) MESSENGER observations of a flux-transfer-event shower at Mercury. J Geophys Res Space Phys. https://doi.org/10.1029/2012JA017926

Slavin JA, Baker DN, Gershman DJ, Ho GC, Imber SM, Krimigis SM, Sundberg T (2018) Mercury's dynamic magnetosphere. In: Anderson BJ, Nittler LR, Solomon SC (eds) Mercury: the view after MESSENGER, Cambridge planetary science. Cambridge University Press, Cambridge, pp 461–496

Slavin JA, Middleton HR, Raines JM, Jia X, Zhong J, Sun W-J, Livi S, Imber SM, Poh G-K, Akhavan-Tafti M, Jasinski JM, DiBraccio GA, Dong C, Dewey RM, Mays ML (2019) MESSENGER observations of disappearing dayside magnetosphere events at Mercury. J Geophys Res Space Phys 124:6613–6635. https://doi.org/10.1029/2019JA026892

Slavin JA, Imber SM, Raines JM (2021) A dungey cycle in the life of Mercury's magnetosphere. In: Maggiolo R, André N, Hasegawa H, Welling DT, Zhang Y, Paxton LJ (eds) Magnetospheres in the solar system. American Geophysical Union AGU, Washington, D.C., pp 535–556

Solomon SC, McNutt RL, Gold RE, Domingue DL (2007) MESSENGER mission overview. In: Domingue DL, Russell CT (eds) The messenger mission to Mercury. Springer, New York, pp 3–39. https://doi.org/10.1007/978-0-387-77214-1_1

Sun W (2023) Lists of magnetopause and bow shock crossings of Mercury by MESSENGER SPACecraft. https://doi.org/10.5281/ZENODO.8298647

Sun W-J, Slavin JA, Fu S, Raines JM, Sundberg T, Zong Q-G, Jia X, Shi Q, Shen X, Poh G, Pu Z, Zurbuchen TH (2015) MESSENGER observations of Alfvénic and compressional waves during Mercury's substorms. Geophys Res Lett 42:6189–6198. https://doi.org/10.1002/2015GL065452

Tenfjord P, Østgaard N, Snekvik K, Laundal KM, Reistad JP, Haaland S, Milan SE (2015) How the IMF by induces a by component in the closed magnetosphere and how it leads to asymmetric currents and convection patterns in the two hemispheres. J Geophys Res Space Phys 120:9368–9384. https://doi.org/10.1002/2015JA021579

Torrence C, Compo GP (1998) A practical guide to wavelet analysis. Bull Am Meteorol Soc 79:61–78

Trávníček PM, Schriver D, Hellinger P, Herčík D, Anderson BJ, Sarantos M, Slavin JA (2010) Mercury's magnetosphere–solar wind interaction for northward and southward interplanetary magnetic field: hybrid simulation results. Icarus 209:11–22. https://doi.org/10.1016/j.icarus.2010.01.008

Winslow RM, Anderson BJ, Johnson CL, Slavin JA, Korth H, Purucker ME, Baker DN, Solomon SC (2013) Mercury's magnetopause and bow shock from MESSENGER magnetometer observations. J Geophys Res Space Phys 118:2213–2227. https://doi.org/10.1002/jgra.50237

Zhao J-T, Zong Q-G, Yue C, Sun W-J, Zhang H, Zhou X-Z, Le G, Rankin R, Slavin JA, Raines JM, Liu Y, Wei Y (2022a) Observational evidence of ring current in the magnetosphere of Mercury. Nat Commun 13:924. https://doi.org/10.1038/s41467-022-28521-3

Zhao J-T, Zong Q-G, Yue C, Zhou X-Z, Liu Z-Y, Sun W-J, Slavin JA, Raines JM, Zhu X-Y (2022b) ULF modulations on plasma environment and coherent waves of Mercury's magnetosphere: MESSENGER's observation. J Geophys. Res. Space Phys. 127:e2021JA030253. https://doi.org/10.1029/2021JA030253

Zhong J, Wan WX, Wei Y, Slavin JA, Raines JM, Rong ZJ, Chai LH, Han XH (2015) Compressibility of Mercury's dayside magnetosphere. Geophys Res Lett 42:10135–10139. https://doi.org/10.1002/2015GL067063

Zhong J, Wei Y, Pu ZY, Wang XG, Wan WX, Slavin JA, Cao X, Raines JM, Zhang H, Xiao CJ, Du AM, Wang RS, Dewey RM, Chai LH, Rong ZJ, Li Y (2018) MESSENGER observations of rapid and impulsive magnetic reconnection in Mercury's magnetotail. Astrophys J Lett 860:L20. https://doi.org/10.3847/2041-8213/aaca92

Publisher's Note

Springer Nature remains neutral with regard to jurisdictional claims in published maps and institutional affiliations.